Numerical analysis of optothermionic refrigeration in semiconductor triple-well structure

Peng Han and Kui-juan Jin[a)]
Beijing National Laboratory for Condensed Matter Physics, Institute of Physics, Chinese Academy of Sciences, Beijing 100080, China

Shang-Fen Ren
Department of Physics, Illinois State University, Normal, Illinois 61790-4560, USA

Yue-liang Zhou and Hui-bin Lu
Beijing National Laboratory for Condensed Matter Physics, Institute of Physics, Chinese Academy of Sciences, Beijing 100080, China

(Received 25 July 2007; accepted 24 September 2007; published online 3 December 2007)

The refrigeration processes in the InP/AlInAs triple-well semiconductor system with various structures are analyzed theoretically based on the model of optothermionic refrigeration. Thermal energy extraction in the triple-well system is calculated to be as much as 26 W/cm^2 theoretically with properly designed well widths and doping densities. Furthermore, the temperature drop distributions for hot semiconductor devices are obtained self-consistently with various parameters including cross-sectional area, generation heat, environment temperature, and refrigeration heat.
 [DOI: 10.1063/1.2817256]

I. INTRODUCTION

With advances in semiconductor laser sources for the telecommunication industry and the increased speed of microprocessors for the computer industry, heat management has become an important issue in the performance of these devices.[1] As an important semiconductor refrigeration method, thermoelectric (also called Peltier) refrigeration has been employed in microelectronic and optoelectronic devices to stabilize the operation of semiconductor devices for many years.[2–4] However, the traditional thermoelectric coolers are used mainly in applications where reliability and convenience are more important than economics due to their poor efficiencies.[2] To go beyond thermoelectric refrigeration, a method of thermionic refrigeration based on the thermal emission of electrons was proposed by Mahan.[3] In thermionic motion, the electrons go over the barrier ballistically so they carry kinetic energy from one electrode to another in a device with a relatively high efficiency. As a result, thermionic refrigeration devices can obtain high refrigeration efficiency.[5] Though the theoretical refrigeration efficiency of thermionic coolers is predicted to be close to the Carnot efficiency,[7] the practical efficiencies are not so high.[7–9] To improve the efficiency of a thermionic refrigerator, considerable efforts have been made such as single barrier heterostructure refrigeration,[8,9] double barrier semiconductor heterostructure refrigeration,[10] semiconductor superlattice refrigeration,[11] and metal-semiconductor multilayer refrigeration.[12,13]

Besides improving the intrinsic thermionic efficiency, Mal'shukov *et al.* proposed the model of *optothermionic* refrigeration, which combines the ideas of laser refrigeration and thermionic refrigeration to quickly extract heat from the thermionic refrigeration system.[14] In their model, a narrow semiconductor well is embedded in the middle of a highly doped *pn* junction. Electrons in the *n* region and holes in the *p* region are thermally excited into the well via the thermionic refrigeration process. In the well region, the electrons and holes can recombine to emit light, so the photons are the media to extract the heat from the system.[14] The laser refrigeration of semiconductors has been proven to be feasible considering the effects of luminescence trapping and redshifting due to the reabsorption of photons.[6] For practical applications of the optothermionic refrigeration, it is important to optimize the design of the semiconductor optothermionic refrigeration systems to achieve the highest possible efficiency.

To obtain a high efficiency refrigeration system, a numerical design of a semiconductor optothermionic refrigeration system has been performed based on the self-consistent calculation.[15,18] In these works, the double-well system was proven as an optimal refrigeration device, and it was predicted that the refrigeration heat is not increased with the further increase of the number of wells. However, the limitation to double wells will limit the feasibility of optothermionic refrigeration devices in real applications due to the limited size of the refrigeration region. In this paper, we report the numerical design of an optothermionic refrigeration device in an $InP/Al_{0.65}In_{0.35}As$ semiconductor triple-well system. Our results show that the refrigeration heat is affected greatly by the well width of the system, and the proper well width for high refrigeration heat is predicted. The results provide a method to further the design of multiple-well optothermionic refrigeration systems. In addition, the temperature drop distributions of the optothermionic refrigeration

[a)]Author to whom correspondence should be addressed. Electronic mail: kjjin@aphy.iphy.ac.cn.

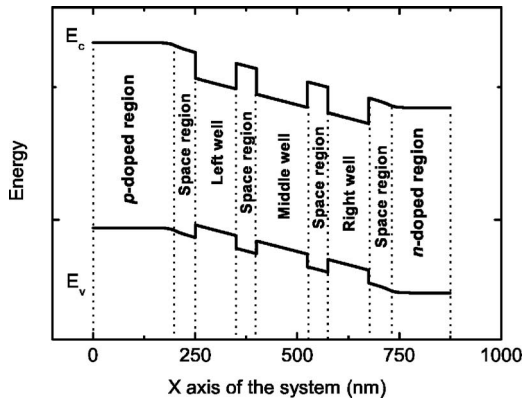

FIG. 1. Schematic band diagram of InP/AlInAs triple-well optothermionic refrigeration system.

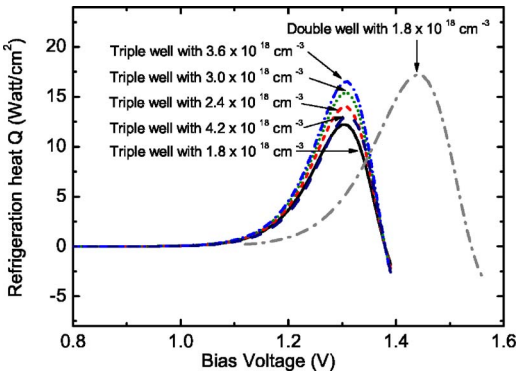

FIG. 2. (Color online) Comparison between the refrigeration heat Q in the triple-well system and in the double-well system with various doping densities. All the well widths are 100 nm.

process over parameters such as cross-sectional area, generation heat, environment temperature, and refrigeration heat are given as examples in this work.

II. TRIPLE-WELL SYSTEM

Optothermionic refrigeration consists of two competing processes: to heat up the system by energy dissipation JV within the sample, where J is the current flow through the system and V is the bias voltage applied on the system; and to cool down the system with light emission heat Q_{rad}.[14] If the *refrigeration heat* Q,

$$Q = Q_{\mathrm{rad}} - JV, \tag{1}$$

is positive, the optothermionic refrigeration can be realized. The detailed expression for refrigeration heat has been given elsewhere,[14,15] and the numerical results of refrigeration heat Q as a function of bias voltage V can be obtained with various semiconductor parameters based on the self-consistent calculation by using the optothermionic refrigeration model, the Poisson equation, and drift-diffusion formulas.[15–17]

For obtaining higher efficiency of optothermionic refrigeration, an InP/$Al_{0.65}In_{0.35}As$ semiconductor triple-well system is designed. The schematic diagram of the triple-well refrigeration system is plotted in Fig. 1. In this cooling device, the p- and n-doped AlInAs alloys act as metal electrodes and the undoped AlInAs layers are used as spacer layers between the pure InP wells and the highly doped AlInAs alloy.

The refrigeration heat curves in the triple-well systems with three 100 nm wells are shown together with a double-well system with two 100 nm wells in Fig. 2. The latter is the optimal design for the double-well system.[18] As shown in this figure, the refrigeration heat Q in the triple-well system is much less than that in the double-well system with same doping density of $N_{\mathrm{imp}}=1.8\times10^{18}$ cm^{-3}, which is the optimal doping density calculated for the double-well system.[18] The refrigeration heat of the triple-well system is increased with the further increase of doping density, and the theoretical optimal refrigeration heat is obtained with a doping density of $N_{\mathrm{imp}}=3.6\times10^{18}$ cm^{-3}. However, as shown in Fig. 2, the refrigeration heat of the triple-well system with the proper doping density is still less than that of the double-well system, and this is consistent with the previous work.[18] For obtaining higher refrigeration heat, we design the triple-well system with various well widths and plot the refrigeration heat curves in Fig. 3. In this figure, the well width of the middle well in the triple-well system is 100 nm for all curves, and the well widths of the left and right wells are 75 nm (solid curve), 100 nm (dashed curve), 125 nm (dotted curve), and 150 nm (dashed dotted curve), respectively. The doping density is kept the same as $N_{\mathrm{imp}}=3.6\times10^{18}$ cm^{-3}. This figure shows that in the triple-well system, the refrigeration heat is increased with the increase of well width and is higher than that in the double-well system when the left and right well width of the triple-well system is 125 nm. However, the refrigeration heat is decreased with further increase of the well width. This behavior can be understood as follows. As shown in Ref. 15, both the size of the refrigeration region and the polarization of the spatial distribution of carriers are increased with the increase of well width. The former increases the refrigeration heat while the latter reduces it. Thus the competition between these two determines the total refrigeration heat.

For the design of more effective optothermionic refrigeration devices, the refrigeration heat curves with various well widths of the middle well are also given in Fig. 4. In

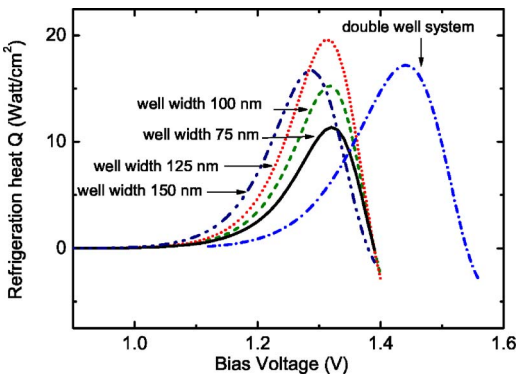

FIG. 3. (Color online) Comparison between the refrigeration heat Q in the triple-well system and in the double-well system. The well widths of the left and right wells in the triple-well system are 75 nm (solid curve), 100 nm (dashed curve), 125 nm (dotted curve), and 150 nm (dashed dotted dotted curve), and the middle well width is 100 nm. The well width of each well in the double-well system is 100 nm.

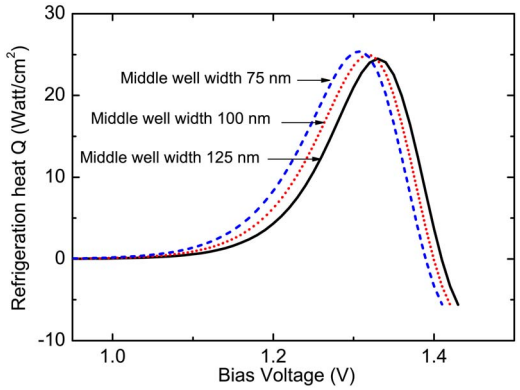

FIG. 4. (Color online) The refrigeration heat Q with various middle well widths in the triple-well system *without* considering the effect of the well width dependent Auger recombination. The well width of the left and right wells is 125 nm.

this figure, the well width of the left and right wells is 125 nm and the middle well widths are 75 nm (dashed curve), 100 nm (dotted curve), and 125 nm (solid curve); the doping density N_{imp} is 3.6×10^{18} cm^{-3}. As shown in the figure, the refrigeration heat is increased with the decrease of the well width of the middle well. However, the decrease of the well width is limited because the nonradiative Auger recombination coefficient is increased with the decrease of well width in the quantum well system,[14,19,20] and the decrease of the recombination coefficient will reduce the refrigeration heat. Considering the effect of the well width dependent Auger recombination process,[19] the calculated refrigeration heat versus bias voltage of the above structures is plotted in Fig. 5. As shown in this figure, the refrigeration heat in the system with the middle well widths of 75 and 100 nm is as high as 26 W/cm^2, while that in the system with 50 nm well width is about 23 W/cm^2. Thus, well widths of 125 nm for the left and right wells and 75 nm for the middle well, together with a doping density N_{imp} of 3.6×10^{18} cm^{-3}, are the theoretically optimized parameters for the triple-well refrigeration system.

III. REFRIGERATION AND TEMPERATURE

Although the plots of refrigeration heat Q versus bias voltage V shown in Figs. 2–5 provide a way to understand

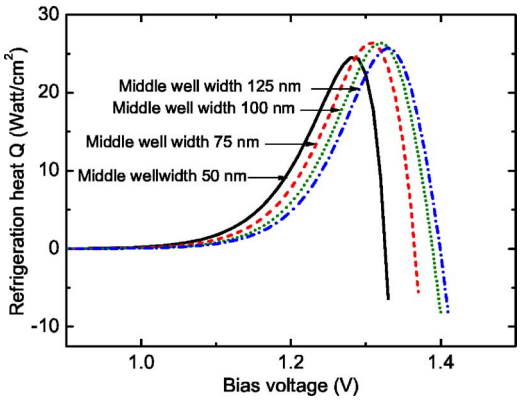

FIG. 5. (Color online) The refrigeration heat Q with various middle well widths in the triple-well system *with* considering the effect of the well width dependent Auger recombination. The well width of the left and right wells is 125 nm.

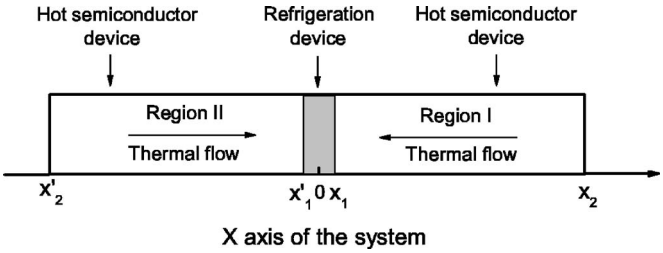

FIG. 6. The schematic of the thermal transport in the real system. The gray part between points x_1 and x_1' is the optothermionic refrigeration device. Region I (x between x_1 and x_2) and region II (x between x_1' and x_2') are the hot semiconductor devices such as microprocessors or semiconductor lasers, respectively. The heat in regions I and II will thermally diffuse into the refrigeration device and will be extracted from the system by photons.

the physical processes, it will be practical and informative to provide the distribution of temperature drop (ΔT) with certain conditions for the real application of optothermionic refrigeration devices.

To describe the refrigeration process in a real system, we introduce a simple model as shown schematically in Fig. 6. In this figure, region I (x between points x_1 and x_2) and II (x between points x_1' and x_2') are the hot semiconductor devices such as microprocessors or semiconductor lasers, which generate the thermal energy of $Q_g(x)$ per unit volume, and a refrigeration device (x between points x_1 and x_1') is embedded between these two regions. Within this model, the optothermionic refrigeration system is viewed as a whole device and extracts thermal energy as $\frac{1}{2}Q$ at its boundary points $x=x_1, x_1$.

When the heat is extracted from the refrigeration device, the hot phonons will thermally diffuse into the refrigeration device from the hot semiconductor devices. This process can be described by the following:

$$C_v(T)\frac{\partial T(x,t)}{\partial t} - \kappa(T)\frac{\partial^2 T(x,t)}{\partial x^2} = Q_g(x) + \frac{4\sigma}{\sqrt{S}}[T_0^4 - T^4(x,t)], \tag{2}$$

where $T(x,t)$ describes the temperature depending on time and position dependence, σ presents the Stefan-Boltzmann constant, T_0 is the constant surrounding temperature, and S describes the cross-sectional area. The unit volume specific heat of semiconductor lattice $C_v(T)$ and the thermal conductivity $\kappa(T)$ can be presented as follows:[21–23]

$$C_v(T) = \sum_{\lambda} C_{\lambda}(T) \tag{3}$$

and

$$\kappa(T) = \frac{1}{3}\sum_{\lambda} C_{\lambda}(T) s_{\lambda}^2 \tau \tag{4}$$

with

$$C_{\lambda}(T) = \frac{1}{V_s k_B T^2}\sum_{q} \frac{(\hbar\omega_{\lambda,q})^2 \exp(\hbar\omega_{\lambda,q}/k_B T)}{[\exp(\hbar\omega_{\lambda,q}/k_B T) - 1]^2}, \tag{5}$$

where V_s describes the volume of the hot semiconductor device, k_B is the Boltzmann constant, and $\hbar\omega_{\lambda,q}$ presents the phonon energy with the wave vector q and the mode λ, λ

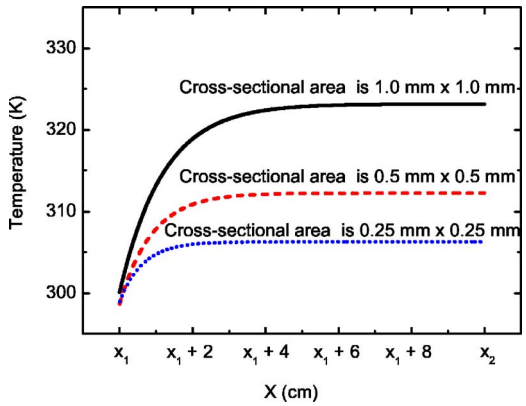

FIG. 7. (Color online) The temperature drop distribution with various square cross-sectional areas in region I (between x_1 and x_2). The environment temperature is 300 K, and the generation heat per unit volume of the hot semiconductor device is 10 W/cm^3.

=TA (transverse-acoustic mode), LA (longitudinal-acoustic mode), TO (transverse-optical mode), and LO (longitudinal-optical mode). s_λ presents the sound velocity for each phonon mode and τ is the average phonon relaxation time. For simplification, we use the material parameters of InP (Ref. 24) in the calculation of the process of thermal transport in regions I and II.

The temperature distribution with position x is calculated by using the above equations. The temperature distribution curves with various square cross-sectional areas of 0.25×0.25 mm^2, 0.5×0.5 mm^2, and 1.0×1.0 mm^2 in region I are shown in Fig. 7. The environment temperature is 300 K and the generation thermal energy per unit volume is 10 W/cm^3. As shown in this figure, the temperature drop is increased with the increase of system temperature. Furthermore, the effect of the environment temperature on the system is decreased with the increase of cross-sectional area. The former is because the refrigeration heat is increased with the increase of temperature, and the latter can be explained as follows: The effect of environment temperature on the system is mainly by thermal radiation, which depends on the surface area of system $4(x_2-x_1)\sqrt{S}$ with the volume of $(x_2-x_1)S$. Thus the thermal radiation heat per unit volume is determined to be $4/\sqrt{S}$, which decreases with the increase of the cross-sectional area.

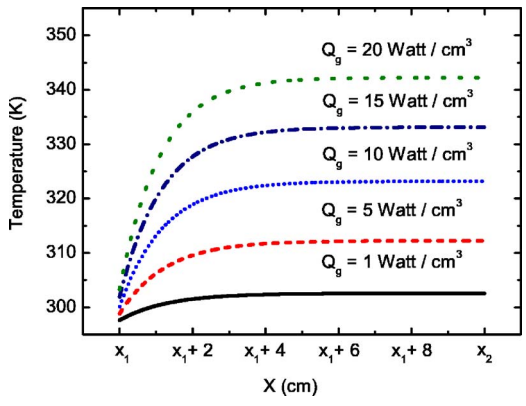

FIG. 8. (Color online) The temperature drop distribution with various generation heats per unit volume of the hot semiconductor devices in region I (between x_1 and x_2). The cross-sectional area is 1.0×1.0 mm^2 and the environment temperature is 300 K.

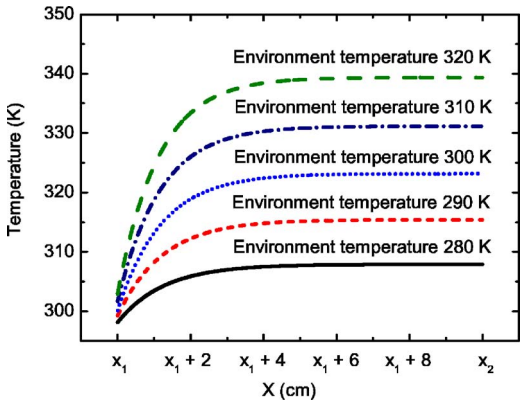

FIG. 9. (Color online) The temperature drop distribution with various environment temperatures in region I (between x_1 and x_2). The cross-sectional area is 1.0×1.0 mm^2 and the generation heat per unit volume of the hot semiconductor device is 10 W/cm^3.

To investigate the effects of the generation heat on the temperature drop, we plot the temperature distribution curves with various $Q_g(x)$ in Fig. 8. In addition, the temperature distribution curves with various environment temperatures are given in Fig. 9. As shown in these figures, the temperature drop is increased with increase of generation heat and environment temperature. These results reveal that the optothermionic refrigeration system is a good candidate for cooling hot semiconductor devices with high generation heat at high environment temperature.

The former discussion is based on the refrigeration heat Q at the ideal maximum value, which is difficult to be obtained in the real system. For real applications, the temperature drop distribution curves with various refrigeration heat Q's such as 0, 5, 15, 20, and 25 W/cm^2 are given in Fig. 10, and these curves will help with the design of the refrigeration system for the hot semiconductor devices.

IV. SUMMARY

In summary, the optimal triple-well semiconductor optothermionic refrigeration systems have been designed self-consistently based on the model of semiconductor optothermionic refrigeration. From our calculation, refrigeration heat

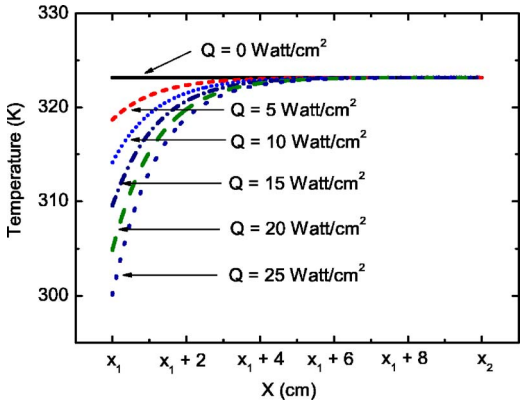

FIG. 10. (Color online) The temperature drop distribution with various refrigeration heats Q in region I (between x_1 and x_2). The environment temperature is 300 K, the cross-sectional area is 1.0×1.0 mm^2, and the generation heat per unit volume of the hot semiconductor device is 10 W/cm^3.

as high as about 26 W/cm^2 is obtained with properly designed semiconductor structures and doping densities in the InP/AlInAs triple-well system. Furthermore, the distribution of temperature drop in hot semiconductor device systems with cross-sectional area, generation heat, environment temperature, and refrigeration heat are given in this work. These results indicate that the semiconductor multiple-well optothermionic refrigeration system has large potential in practical applications for cooling microprocessors and semiconductor laser devices.

ACKNOWLEDGMENTS

This work is supported by a grant from the National Natural Science Foundation of China.

[1]B. C. C. Lough, Ph.D. thesis, University of Wollongong, 2004.
[2]G. D. Mahan, B. C. Sales, and J. Sharp, Phys. Today **50**, 42 (1997).
[3]G. D. Mahan, in *Solid State Physics*, edited by H. Ehrenreich and F. Spaepen (Academic, New York, 1998), Vol. 51, p. 81.
[4]C. B. Vining and G. D. Mahan, J. Appl. Phys. **86**, 6852 (1999).
[5]G. D. Mahan, J. O. Sofo, and M. Bartkowiak, J. Appl. Phys. **83**, 4683 (1998).
[6]M. Sheik-Bahae and R. I. Epstein, Phys. Rev. Lett. **92**, 247403 (2004).
[7]G. D. Mahan, J. Appl. Phys. **76**, 4326 (1994).
[8]A. Shakouri and J. E. Bowers, Appl. Phys. Lett. **71**, 1234 (1997).
[9]A. Shakouri, C. Labounty, J. Piprek, P. Abraham, and J. E. Bowers, Appl. Phys. Lett. **74**, 88 (1999).
[10]B. C. Lough, S. P. Lee, R. A. Lewis, and C. Zhang, Physica E (Amsterdam) **11**, 287 (2001).
[11]J. Z. Zhang, N. G. Anderson, and K. M. Lau, Appl. Phys. Lett. **83**, 374 (2003).
[12]G. D. Mahan and L. M. Woods, Phys. Rev. Lett. **80**, 4016 (1998).
[13]A. G. Mal'shukov, Z. Ma, V. B. Antonyuk, and K. A. Chao, Solid State Commun. **119**, 563 (2001).
[14]A. G. Mal'shukov and K. A. Chao, Phys. Rev. Lett. **86**, 5570 (2001).
[15]P. Han, K-j. Jin, Y. Zhou, X. Wang, Z. Ma, S. F. Ren, A. G. Mal'shukov, and K. A. Chao, J. Appl. Phys. **99**, 074504 (2006).
[16]K. Horio and H. Yanai, IEEE Trans. Electron Devices **37**, 1093 (1990).
[17]M. S. Lundstrom and R. J. Schuelke, IEEE Trans. Electron Devices **30**, 1151 (1983).
[18]P. Han, K-j. Jin, Y-l. Zhou, H-b. Lu, and G-z. Yang, J. Appl. Phys. **101**, 014506 (2007).
[19]A. S. Polkovnikov and G. G. Zegrya, Phys. Rev. B **58**, 4039 (1998).
[20]M. I. Dyakonov and V. Yu. Kachorovskii, Phys. Rev. B **49**, 17130 (1994).
[21]P. L. Taylor and O. Heinonen, *A Quantum Approach to Condensed Matter Physics* (Cambridge U. P., Cambridge, 2002).
[22]S. F. Ren, W. Cheng, and G. Chen, J. Appl. Phys. **100**, 103505 (2006).
[23]D. Huang, T. Apostolova, P. M. Alsing, and D. A. Cardimona, Phys. Rev. B **70**, 033203 (2004); **72**, 195308 (2005).
[24]The material parameters of InP are obtained from http://www.ioffe.ru/SVA/NSM/Semicond/InP/electric.html